ORBITAL AND INTERANNUAL VARIABILITY OF THE GLOBAL MARS ATMOSPHERE. R.T. Clancy, Space Science Institute, P.O. Box 3075, Bald Head Island, NC 28461, clancyr@colorado.edu

Introduction: Studies of the Mars atmosphere over the past twenty years are largely based on a diverse set of Viking surface and atmospheric measurements collected between 1976-1981. The Viking-based view of the Mars atmosphere synthesized from these data is characterized by a constant background of vertically well mixed dust aerosol ($\tau \geq 0.5$), which increases by factors of ≥3 during the perihelion dust storm season [1]. Low-to-mid latitude atmospheric temperatures in all seasons are typically elevated by >15 K due to solar absorption by the suspended dust [2]. The global distribution of the atmospheric water column exhibits strong annual variation, which is primarily due to annual release of water from the exposed water ice residual cap and the receding CO_2 seasonal ice cap of the northern summer hemisphere. Polar sources of water vapor in the southern summer hemisphere are determined to be much smaller [3]. The warm atmospheric temperatures of the Viking model yield sub-saturation conditions for water vapor in the low-to-mid latitude atmosphere, to altitudes above 25 km in all seasons. As a result, Mars atmospheric photochemistry is characterized by high levels of catalytic radicals from water vapor photolysis (HO_x), and ice cloud formation is restricted to local phenomena (nighttime surface haze, topographic and wave driven discrete clouds) at low-to-mid latitudes. In the context of the Viking model, water ice clouds are not considered to influence the dynamical/radiative balance of the global Mars atmosphere [3].

A revision of this Viking-based climatology is merited on several accounts. The accumulation of ground-based and spacecraft observations over the past decade may be compared to the Viking and Mariner 9 observations to characterize the interannual variation of the Mars atmosphere in unprecedented detail. In addition, there are indications that the annual behavior of the global Mars atmosphere may not be well represented by the Viking model. Since 1988, ground-based millimeter observations (temperature and water profiling- [4,5]) and HST ultraviolet-visible imaging and spectroscopy [6-10] have determined colder (15-20K), cloudy, and less dusty conditions for the global Mars atmosphere relative to the Viking climatology, particularly for the minimum solar heating conditions around aphelion. Clancy et al. [5] identified a distinctive equatorial cloud belt in HST imaging during Mars aphelions in 1991, 1993, and 1995 (figure 1), and associated this phenomenon with the low altitudes (<10 km) of global water saturation and the latitudinal dependence of Hadley vertical advection during the northern summer season of aphelion (solar longitudes, L_s, of 40-140°). They further proposed that ice growth on dust aerosols leads to nonlinear feedback among atmospheric water vapor, temperature, cloud and dust distributions within the Mars atmosphere [11], and results in a much stronger orbital variation of the global Mars atmosphere than is reflected in the existing Viking climatology.

In the past two years, atmospheric measurements from Pathfinder [12,13] and Mars Global Surveyor [14-18], and reanalyses of Viking IRTM observations [18-20] have provided critical cross comparisons to contemporaneous ground-based observations and a reappraisal of atmospheric conditions that existed during the Viking period. These results are integrated with prior spacecraft and ground-based measurements to construct a revised description of the average annual variation of the Mars atmosphere, and a preliminary description of its interannual variability. Ultimately, MGS and the Mars Climate Observer (MCO) will define the spatial and seasonal variation of the global Mars atmosphere in detail that only dedicated atmospheric sounding from orbit can provide. A revision to the Viking model serves to consolidate the significant observational and data analysis developments over the past decade, and provide an interannual context of comparison for the flood of MGS and MCO atmospheric observations that has just begun.

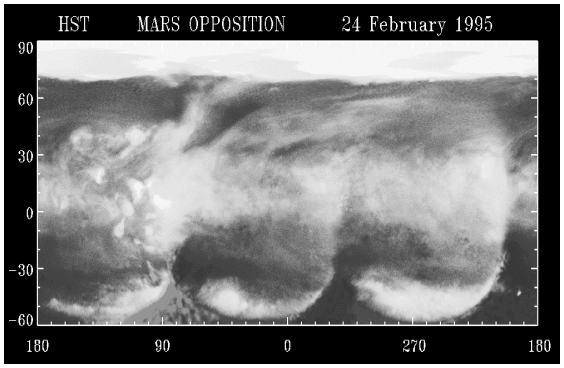

Figure 1: The aphelion global cloud belt in 1995

Atmospheric Temperatures: Figure 2 (from [18]) presents a broad comparison of observed low-to-mid latitude average temperatures at the 0.3 mbar pressure level (~30 km) versus Mars season. Temperature variations at this level are fairly representative of observed behavior over the extended Mars atmosphere (5-50 km), and can be compared among many data sets. For the purpose of these compari-

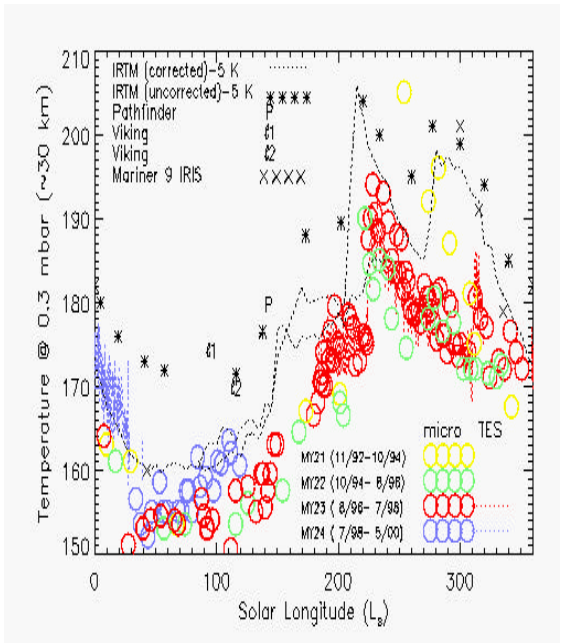

Figure 2: Orbital and interannual variations of low-to-mid latitude Mars atmospheric temperatures

sons, a solar longitude range 0-360° defines a Mars year, and April 11, 1955 (L_s=0°) is adopted as the beginning of year 1. In this arbitrary convention, the Mariner 9, Viking, Phobos, and Pathfinder missions occurred in years 9-10, 12-15, 19-20, and 23 respectively. By comparison, the 1992-1999 millimeter observations (circles, [5,18]) extend over years 21-24, and the 1997-1999 TES observations (dotted lines, [16]) over portions of years 23 and 24. The millimeter and TES measurements show excellent agreement over the 1997-1998 (L_s=190-30°) period of contemporaneous observations. The "uncorrected" IRTM temperatures (asterisks, [21]), which characterize the Viking model of Mars atmospheric behavior, fall 15 K above the temperatures retrieved by the millimeter measurements in all seasons. The "corrected" IRTM temperatures (dotted lines), resulting from the Wilson and Richardson [19] reanalysis of IRTM 15 μm radiances, are reasonably consistent with the seasonal and interannual dependence of atmospheric temperatures displayed by the millimeter measurements. It is also notable that the corrected 15 μm IRTM measurements of 20-30 km atmospheric temperatures are now 10-15K colder than the two Viking descent temperature profiles at L_s=96° and 116°. A similar conflict exists between the cold millimeter profiles and the warm Pathfinder descent temperature profile at L_s=140° in 1997 [18,22]. Within the millimeter data set, interannual variations in global-average atmospheric temperatures (by 5-20 K) are most prominent during the perihelion dust storm season (L_s=200-340°) and during the northern summer/fall period (L_s=100-200°). These are the same seasons for which millimeter and corrected IRTM temperatures exhibit their largest differences (10-20 K).

Global temperature increases associated with the onset of perihelion dust storms have been observed in the millimeter record in four consecutive Mars perihelions (years 20-23). Temperature increases of 15 K retrieved from millimeter and TES observations during the L_s=225° Noachis Terra regional dust storm in 1997 (year 23) are remarkably similar to the L_s=220° temperature increase in 1995 (year 22). However, the 25-30 K elevation of global temperatures determined from the L_s=254° millimeter measurement in 1995 (year 21) is more comparable to temperature increases which accompanied the Mariner 9 (year 9, [23]) and Viking (year 12) global dust storms. The detection of 4-5 small (5-10 K), yet distinct global temperature increases during the 1997 perihelion period suggests a fairly continuous spectrum of dust storm size and atmospheric forcing.

The early aphelion period (L_s=10-90°) presents the greatest degree of repeatability in Mars atmospheric temperatures, in terms of variability within the long-term millimeter data set and in comparison between the corrected IRTM and millimeter observations. Millimeter observations of aphelion atmospheric temperatures exist for years 14, 15, and 19-24. With the Wilson and Richardson correction for the Viking IRTM 15 μm radiances, all eleven observed Mars aphelions over the period year 9 to year 24, including the Mariner 9 period, have exhibited comparably cold atmospheric temperatures (to within 5 K) at this altitude level.

Dust and Ice Opacities: Figure 3 presents a comparison of visible dust column opacities at 0-30 N latitudes as derived from Mariner 9 IRIS (filled triangles-[24]) 9 μm dust opacities (1972, scaled by a factor-of-two); Viking lander 1 (+'s in year 12, X's in year 13-[1]) solar extinction measurements (1976-78); Viking IRTM (filled squares in year 12, filled diamonds in year 13-[25]) 9 μm dust opacities (1976-78, scaled by a factor-of-two); 1989 Phobos (asterisk) solar occultation [26]; 1995-97 Hubble Space Telescope imaging (HST-open triangles in years 20-22, open squares in year 23-[8]) imaging; and Pathfinder solar extinction imaging (solid line-[13]). Included in this figure are the average TES 9 μm dust opacities for the 0-30N latitude range in 1997-98 (filled circles-[15]), which have been scaled by a factor-of-two to present comparable visible dust opacities. Afternoon dust opacities from the Viking 1 lander

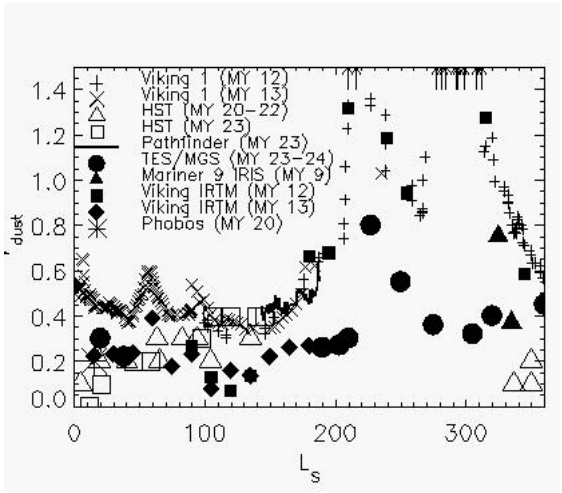

Figure 3: Orbital and interannual variations of low latitude dust opacity in the Mars atmosphere

record (smoothed with a running five point average) are presented, and the Viking and Pathfinder opacities are scaled to a surface pressure of 6.1 mbar (as are the TES opacities).

To first order, the Mars atmosphere in 1996-1998 (years 22-23) shows significantly lower dust loading relative to the 1976-77 Viking period (year 12). At L_s of 190-320° the 1997-98 TES measurements imply visible dust opacities at northern low latitudes which are 2-8 times lower than during the Viking period. TES dust measurements prior to the Noachis Terra storm show a factor of 2-3 less dust loading, compared to Viking 1 lander and IRTM measurements prior to the 1977a storm (0.3 versus 0.6-0.8 at L_s=180-205°. Notice, however, IRTM opacities at L_s=180-185° are significantly lower in year 13 than in year 12). Perihelion dust storm loading was particularly lower in 1997-98 relative to the 1977 period. The Noachis Terra dust storm of 1997 led to relatively modest dust loading in the northern hemisphere [13,14], as compared to the large dust opacities observed by both Viking landers and IRTM during the 1977a and 1977b dust storms (visible dust opacities of 0.6-0.8 versus 2-4). Although there are 30-50% increases in TES dust opacities between L_s=300° and 360° (which correspond to distinct L_s=310° and 340° atmospheric heating events, see figure 2), there was no second dust storm in 1997-98 comparable to the 1977b storm. Consequently, the L_s=280-320° seasonal range was much less dusty (3-8 times) in year 23 than during the equivalent season in year 12. Similarly, this season was less dusty than after the 1971 great dust storm (year 9-c.f., TES and IRIS), although by L_s=330-340° the 1972 dust loading had decayed to comparable levels observed in 1998.

The L_s=350-180° period of northern spring/summer exhibits a more complex variation among the TES, Viking

lander and IRTM, HST, and Phobos dust opacity measurements. At L_s=360° TES measurements are 2-3 times larger than the HST opacities, but are in reasonable agreement with the dust columns measured by Viking 1 and IRTM in 1977. However, the L_s=300-360° period in 1998 presents an increasing dust column due to the late season dust storm events at L_s=310° and 340° (figure 5). By comparison, the Viking 1977 and Mariner 9 1972 dust opacities over this L_s range decreased by a factor of 2-4, associated with the decay of the 1977b and 1971 storms. The TES opacities at L_s=20-40° are comparable to the Phobos (year 20), HST (years 20-23), and Viking IRTM (years 12-13) measurements for this season (τ_{vis}~0.1-0.3), and roughly a factor of 2 less than the Viking lander 1 opacities. The northern summer season at L_s=140-180° shows good agreement among the Viking lander and Pathfinder observations, whereas the Viking IRTM and MGS TES measurements in 1976-78 and 1997 are typically lower by a factor-of-two.

The differences between the 1978 Viking lander and IRTM opacities over L_s=10-180° (year 13) and the 1997 TES and Pathfinder measurements at L_s=190° (year 23) are particularly surprising as these are contemporaneous data sets. The unrecognized contribution of large aphelion cloud opacities in the lander aerosol measurements may account for much of this disagreement. The lander analyses effectively assume negligible cloud opacities during the daytime, consistent with the Viking-based model of a warm, dusty atmosphere, whereas the IR measurements spectroscopically discriminate cloud and dust opacities. HST imaging during the past 5 aphelions (years 20-24) clearly identifies the presence of daytime cloud opacities of 0.1-0.4 (figure 1). The Wilson and Richardson [19] reanalysis of Viking IRTM 15 μm measurements (figure 2) now implies comparable aphelion saturation conditions for the Viking period, and recent analysis of IRTM 11 μm radiances identifies the presence of a global aphelion cloud belt during the Viking period (Tampari et al., 1997). Finally, TES mapping of dust and ice opacities during the 1999 aphelion (L_s=110°) provides a striking display of the aphelion cloud belt in the 11-12 μm water ice band [17]. These TES measurements imply that visible cloud opacities can exceed visible dust opacities (τ_{dust}~0.1) within the aphelion cloud belt.

It is also worth noting the possibility that fine CO_2 ice clouds may be a relatively common low latitude phenomenon within the mesosphere (60-100 km altitudes) of Mars. Submillimeter measurements of temperatures at the 70-80 km altitude region indicate dayside average temperatures only 10 K above CO_2 saturation conditions during the equinoctal seasons [22]. The presence of CO_2 ice clouds in the mesosphere was proposed as an explanation of the 4.3 μm CO_2 ice spectral line scattering identified by Mariner 6 and 7 IRS limb observations at L_s=200° in 1969 [32]. In addition, very cold regions over the 60-90 altitude range were observed to fall below CO_2 saturation conditions during the Pathfinder descent [12].

Water Vapor and Photochemistry: Figures 4 and 5 present two aspects of Mars atmospheric water behavior which may be considered as significant modifications to the Viking model. In figure 4, the latitudinal dependence of Mars atmospheric water column during the northern vernal equinox is presented for four separate Mars years. This comparison of Viking MAWD observations [27] to recent ground-based visible [28,29] and centimeter [30] measurements provides one of the more compelling cases for strong interannual variability of Mars atmospheric water. A factor of >4 interannual variation is implied over the 1988-1994 period for this season of minimum atmospheric water abundance [29,30]. By comparison, ground-based and Viking observations during the northern spring/summer season of maximum atmospheric water abundance (L_s=20-120°) show relatively modest interannual variability [29,31].

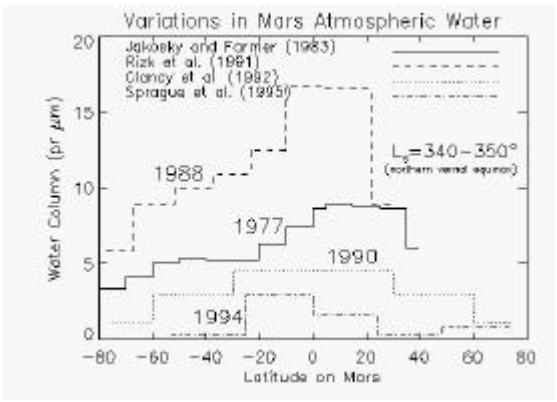

Figure 4: The interannual variation of Mars atmospheric water in late northern winter

Figure 5 presents the behavior of water vapor saturation conditions in the low-to-mid latitude Mars atmosphere as a function of season [5]. The colder atmospheric conditions returned by the millimeter observations (dashed lines, computed for 3 levels of atmospheric water abundance) lead to much lower altitudes of water saturation relative to the Viking climatology (solid lines). Differences between these models in the perihelion season reflect interannual variability of dust storm activity in this season. TES observations show correlations in 30-50 km water clouds with dust storm activity in this season in 1997 [17]. Differences between the Viking and microwave (millimeter) based models during the aphelion period are a consequence of the warm bias in the Viking model (figure 2). Millimeter HDO and centimeter H_2O spectral line observations confirm the presence of very low saturation altitudes around 1993 and 1995 Mars aphelions [5]. The resulting orbital variation in water vapor densities at altitudes above 10 km forces large orbital variations in atmospheric photochemistry [33], as water photolysis products (OH, HO_2, H_2O_2) are the primary catalytic reagents for ozone destruction in the Mars atmosphere [32]. HST

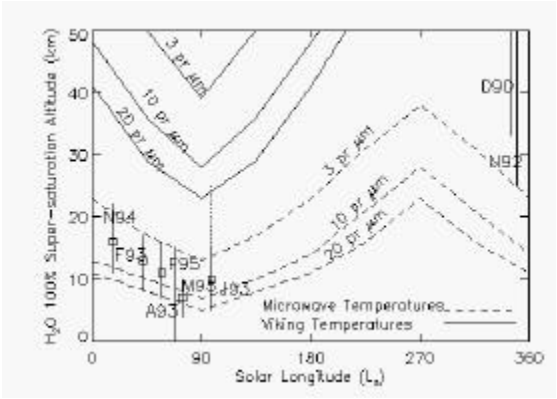

Figure 5: Orbital variation of low-to-mid latitude water vapor saturation conditions in the Mars atmosphere

ultraviolet spectroscopic determinations of Mars ozone column distributions show that low-to-mid latitude ozone column increases by a factor-of-two during the aphelion period [9,10]. This increase in the ozone column corresponds to factors of 3-10 in ozone density increases above 10 km altitudes, which result from the removal of vapor vapor by saturation and cloud formation around the aphelion season [33].

Revised Atmospheric Climatology: The strong (40%) orbital variation in solar flux incident on Mars leads to distinct aphelion and perihelion climates, which occur (in the current epoch) around the northern and southern summer solstices, respectively. Annual variations in the general circulation of the atmosphere and the growth/recession of the polar caps are more closely tied to the obliquity of Mars. In contrast, annual and interannual variations of low-to-mid latitude temperatures, dust and ice aerosol loading, and composition (water, ozone) are more closely tied to aphelion-perihelion orbital variations. The following summary of annual and interannual variations in the global Mars atmosphere employs this orbital methodology.

1) The perihelion season (L_s=200-340°) experiences regional-to-global dust storms every Mars year. Average global dust opacities are significantly reduced during years of regional (τ_{vis}=0.5-1.0) versus global (τ_{vis}=2-4) dust storms. Global dust storms (as in 1971 and 1977) may occur in roughly one-half to one-third of Mars years. Multiple dust storms of smaller extent also occur throughout the L_s=200-340° period. In all cases, from global to sub-regional scale, these dust storms onset as discrete events, leading to 5-30 K global increases in atmospheric temperatures over extended altitudes (0-50 km) and with remarkably abrupt timescales (1-2 days). Atmospheric water abundances in this southern solstice season are several times less than observed during the northern summer solstice. However, they are also poorly determined from existing observations, and may or may not show influences from south polar reservoirs and significant interannual variability. Large (200%) enhancements in water columns appear within the Hellas and Argyre basins over L_s=245-275°, and may strongly influence the latitudinal distribution of atmospheric water in this season. The warm atmospheric conditions of the perihelion period present subsaturation conditions for atmospheric water to high altitudes (35-60 km, where variable, optically thin water ice clouds are present), high levels of photochemical radicals (such as NO_x and HO_x), and minimum levels of atmospheric ozone.

2) The aphelion atmosphere (L_s=20-140°) is most repeatable in temperature, water column, and aerosol conditions from year-to-year. The long-standing Viking model of atmospheric temperature, cloud, and dust behavior is an inaccurate description of this season in particular, even for the Viking period of observation. The aphelion period is characterized global conditions of cold atmospheric temperatures (20-30 K cooler than during perihelion), low altitudes of water vapor saturation (<10 km), enhanced cloud opacities (τ_{vis} = 0.1-0.5, including a distinctive low latitude cloud belt), and low dust opacities (τ_{vis} = 0.1-0.3). As the northern summer season progresses beyond L_s=100°, dust and cloud opacities remain similar to aphelion conditions but atmospheric temperatures exhibit increased temporal (and possibly spatial) variability relative to the L_s=20-100° period. The global distribution of atmospheric water vapor in this season is dominated by northern residual and seasonal cap sources, and does not appear to exhibit strong interannual variability. The low altitudes of global water saturation in this season lead to minimum levels of photochemical radicals and maximum columns of atmospheric ozone (apart from the polar regions).

3) The transitional seasons of L_s=340-20° (northern vernal equinox) and L_s=140-200° (southern vernal equinox) are characterized by intermediate interannual variability in global atmospheric temperatures (5-15 K), relative to the constant aphelion and highly variable perihelion periods. Year-to-year variations of temperature (5-10 K) and dust conditions (τ_{vis}=0.1-0.6) within the L_s=340-20° period reflect year-to-year variations in late perihelion season dust storm activity. Atmospheric water vapor exhibits very large interannual variations during this period (average water columns of ~1 to >10 pr μm), and may indicate comparable interannual variability in southern hemispheric water during the perihelion season when the behavior of atmospheric water is not well observed. Cloud opacities begin to increase and descend to lower altitudes.

Year-to-year variations in global atmospheric temperatures over the L_s=140-200° period are characterized by a distinctive 10-15 K increase in 20-30 km atmospheric temperatures at L_s=140-150° in 1976 and 1978. This behavior is not evident in the 1992-1998 millimeter observations, but current millimeter observations show a trend towards such warmer conditions by L_s=120° in 1999. No obvious increase in dust column opacity accompanies this late northern summer rise in global atmospheric temperatures, suggesting that an increasing vertical extent of the dust heating may contribute to this behavior. This behavior may also reflect an increasing altitude for the formation of water ice clouds, which may still present signifcant opacities. Very cold atmospheric temperatures at 60-100 km altitudes may also lead to local formation of CO_2 ice clouds during the equinoxes.

References: **[1]** Colburn et al. (1989) *Icarus*, 79, 159-189. **[2]** Pollack et al. (1979) *JGR*, 84, 2929-2945. **[3]** Jakosky and Haberle (1992) *MARS*, ed. Kieffer et al, 1151–1154969-1016. **[4]** Clancy et al. (1990) *JGR*, 95, 14543-14554. **[5]** Clancy et al. (1996) *Icarus*, 122, 36-62. **[6]** James et al. (1994) *Icarus*, 109, 79-101. **[7]** James et al. (1996) *JGR*, 101, 18883-18890. **[8]** Wolff et al. (1999) *JGR*, in press. **[9]** Clancy et al. (1996) *JGR*, 101, 12777-12783. **[10]** Clancy et al. (1999) *Icarus*, 138, 49-63. **[11]** Rodin et al. (1999) *Icarus*, in review. **[12]** Schofield et al. (1998) *Science*, 278, 1752-1758. **[13]** Smith et al. (1998) *Science*, 278, 1758-1768. **[14]** Christensen et al. (1998) *Science*, 279, 1692-1698. **[15]** Smith et al. (1999) submitted to *JGR*. **[16]** Conrath et al. (1999) submitted to JGR. **[17]** Pearl et al. (1999) submitted to *JGR*. **[18]** Clancy et al. (1999) submitted to *JGR*. **[19]** Wilson and Richardson (1999) *JGR*, in review. **[20]** Tamppari et al. (1996) *Bull. Amer. Astron Soc*. 29, 961. **[21]** Kieffer et al. (1977) *JGR*, 82, 4249-4292. **[22]** Clancy and Sandor (1998) *GRL*, 25, 489-492. **[23]** Conrath (1975) *Icarus*, 24, 36-46. **[24]** Fenton et al. (1997) *Icarus*, 130, 115-124. **[25]** Martin (1986) *Icarus*, 66, 2-21. **[26]** Chassefiere et al. (1992) *JGR*, 100, 5525-5540. **[27]** Jakosky and Farmer (1982) *JGR*, 87, 2999-3019. **[28]** Rizk et al. (1991) *Icarus*, 90, 205-213. **[29]** Sprague et al. (1995) *JGR*, 101, 23229-23241. **[30]** Clancy et al. (1992) *Icarus*, 100, 48-59. **[31]** Jakosky and Barker (1984) *Icarus*, 57, 322-334. **[32]** Herr and Pimental (1970) *Science*, 167, 47-49. **[33]** Clancy and Nair (1996) *JGR*, 101, 12785-12790. **[34]** Parkinson and Hunten, (1972), *J. Atmos. Sci.*, 29, 1380-1390.